HHS Public Access

Author manuscript

Science. Author manuscript; available in PMC 2018 October 13.

Published in final edited form as:

Science. 2017 October 13; 358(6360): 218–223. doi:10.1126/science.aan7969.

Scalable synthesis of bryostatin 1 and analogs, adjuvant leads against latent HIV

Paul A. Wender[1,2,*], **Clayton T. Hardman**[1], **Stephen Ho**[1], **Matthew S. Jeffreys**[1], **Jana K. Maclaren**[3], **Ryan V. Quiroz**[1], **Steven M. Ryckbosch**[1], **Akira J. Shimizu**[1], **Jack L. Sloane**[1], and **Matthew C. Stevens**[1]

[1]Department of Chemistry, Stanford University, Stanford, CA 94305, USA

[2]Department of Chemical and Systems Biology, Stanford University, Stanford, CA 94305, USA

[3]Stanford Nano Shared Facilities, Stanford University, Stanford, CA 94305, USA

Abstract

Bryostatin 1 is an exceedingly scarce marine-derived natural product that is in clinical development directed at HIV/AIDS eradication, cancer immunotherapy, and the treatment of Alzheimer's disease. Despite this unique portfolio of indications, its availability has been limited and variable, thus impeding research and clinical studies. Here, we report a total synthesis of bryostatin 1 that proceeds in 29 total steps (19 in the longest linear sequence, >80% average yield per step), collectively produces grams of material, and can be scaled to meet clinical needs (~20 grams per year). This practical solution to the bryostatin supply problem also opens broad, facile, and efficient access to derivatives and potentially superior analogs.

Bryostatin 1 is in clinical trials as a first-in-class latency reversal agent for the eradication of HIV/AIDS (1–3). It has also been advanced as a treatment for Alzheimer's disease (4–6) and as an immunotherapeutic agent against cancer (7–9). These diseases represent leading causes of death, affecting hundreds of millions of patients and caregivers. Bryostatin 1's putative target, protein kinase C (PKC), has also been implicated in preclinical studies directed at the treatment of various unmet neurological and cardiovascular indications (10).

Notwithstanding its current and potential clinical use, the National Cancer Institute's (NCI's) limited stock of bryostatin 1 (originally 18 g) is nearly depleted after supplying more than 40 clinical trials in oncology and Alzheimer's disease. This longstanding scarcity of material has severely limited both research and clinical studies (11) and, more generally, has hampered efforts to access potentially superior derivatives and analogs.

*Corresponding author. wenderp@stanford.edu.

SUPPLEMENTARY MATERIALS

www.sciencemag.org/content/358/6360/218/suppl/DC1

Materials and Methods

Figs. S1 to S3

Tables S1 to S4

References (55–78)

Several approaches to solving bryostatin's supply problem have been pursued since its first isolation in 1968 (12, 13). The NCI's original "hand collection" of 14 tons of the marine source organism *Bugula neritina* provided only 18 g of bryostatin 1 (0.00014% yield) (14). Improvements in the extraction of bryostatin 1 from its marine source using supercritical CO_2 have been reported (15) but are ultimately limited by its low and variable natural production and the challenges of sustainable, large-scale harvesting in the delicate and changing marine ecosystem (16). Related efforts to boost production of bryostatin 1 by aquaculture of *B. neritina* were intensely pursued but later abandoned because of large capitalization costs for "in-sea" culture and low natural product yields for "in-tank" culture (17).

As an alternative to marine harvesting, synthetic biological approaches have been reported but remain in early stages because cultivation of the symbiotic bacterium associated with bryostatin production is difficult (18, 19). Representing a third supply strategy, chemical syntheses of various members of the bryostatin family have improved over the years, from as many as 90 steps to as few as 36 steps (20–26). The only reported synthesis of bryostatin 1 required 57 steps (24).

Here, we report a solution to the bryostatin 1 supply problem in the form of a step-economical, multigram-producing synthesis that addresses both clinical and research needs and serves additionally as a practical platform for accessing new and potentially superior analogs. Our convergent synthesis proceeds in 29 steps, with a longest linear sequence (LLS) of 19 steps and 4.8% overall yield (>80% average yield per step), and has collectively produced >2 g of bryostatin 1. All steps, except the final step for safety reasons, were conducted on a gram to multigram scale. This synthesis can thus readily supply the amount of material needed to further advance clinical evaluation, as a single gram of bryostatin 1 can treat ~1000 cancer patients (9, 11) or ~2000 Alzheimer's patients (4) according to currently used clinical dosing.

The synthetic challenge posed by bryostatin 1 is defined in part by its macrocyclic lactone structure, which incorporates three embedded hydropyran rings, 11 stereocenters, and a formidable array of multiple alkene, alcohol, ether, hemiketal, and ester functionalities. Our approach to this challenge (Fig. 1) was inspired by our earlier syntheses of bryostatin 9 (25) and analogs (27–29) and is designed to initially produce in parallel the less complex A- and C-ring subunits of the target. These precursors are then conjoined through a Yamaguchi esterification and Prins macrocyclization to produce the B-ring and, after four subsequent steps, bryostatin 1. An additional advantage of this convergent strategy is that either subunit or final-stage intermediates can be modified to access derivatives and analogs.

The synthesis of bryostatin's C-ring subunit (Fig. 2, aldehyde **2**), which incorporates C15 to C26 of the macrocycle and important structural elements that influence its PKC affinity (30), started with the hydrolysis and in situ prenylation of inexpensive dihydropyran **3** ($3/mol) to form known diol **4** (>20 g scale) (31). This and all subsequent reactions were conducted on multiple scales by multiple investigators to ensure reproducibility and information transfer. Further, although all isolable products were purified and characterized, many steps were designed to be conducted without product purification to reduce time, cost, and waste-

generating chromatographies. As such, crude diol **4** was doubly oxidized to afford 1,5-ketoaldehyde **5** (>25 g scale, 81% yield), setting the stage for C-ring formation. Although previously unexplored on dicarbonyl compounds, Nokami's crotylation procedure involving ketoaldehyde **5** and crotyl transfer reagent **6** (32) was found to proceed with high chemo- and enantioselectivity to set the C23 stereochemistry in alcohol **7** [>98% enantiomeric excess (ee)]. This process can be conducted in one flask along with an in situ cyclodehydration and enol ether epoxidation to yield pyran **9** as a 2:1 inconsequential mixture of C20 epimers. Pyran **9** proved to be unstable and was thus directly oxidized to provide the isolable C20 ketone **10** (69% yield from ketoaldehyde **5**). Compound **10** is the first intermediate in the sequence that required chromatographic purification.

The C-ring enoate of bryostatin 1 was introduced using a one-step aldol condensation protocol, which afforded exclusively the *E*-isomer **12** in 84% yield (27). The C20 ketone was then selectively reduced and esterified to afford octynoate **13**. The introduction of the octynoate at C20 as a less reactive, masked equivalent of the target octadienoate was designed to enable the projected chemoselective oxidation of three different alkenes (see below). This approach was predicated on the ambitious expectation that an yne-to-diene isomerization could be effected on an advanced intermediate at the end of the synthesis.

The first test of our serial alkene oxidation plan was encountered with the dihydroxylation of the C25/C26 alkene in **13** in the presence of two other alkenes and the alkynoate. With Sharpless' cinchona-based system, this reaction proceeded with remarkable stereo-, regio-, and chemoselectivity, oxidizing only one of the four π-systems. The crude diol was directly protected to afford acetonide **14** in 88% yield (over two steps) and 11:1 diastereomeric ratio (dr). Cleavage of the sterically congested but more electron-rich C16/C17 alkene in **14** provided a second test of our plan. Gratifyingly, a stoichiometric ozonolysis reaction resulted in chemoselective cleavage of the C16/C17 alkene to afford aldehyde **15** in 93% yield (25).

The homologation of aldehyde **15** has been a longstanding chemoselectivity challenge because of its steric encumbrance (including unanticipated long-range effects arising from the C25/C26 protecting group) (33–35) as well as the potential for competing deprotonation and Michael additions involving the ynoate and unsaturated ester moieties. Of the many nonbasic nucleophiles we surveyed [including vinyl zinc (36) and cerium (37) reagents], only vinyl zincate **16** cleanly engaged the C17 aldehyde to afford aldehyde **18** (78% yield) after in situ hydrolysis. Subsequently, the C25/C26 acetonide and C19 ketal groups were removed and the C26 alcohol protected to afford aldehyde **2**. Overall, this route to bryostatin's Cring subunit, **2**, proceeded in 13 steps (LLS) and a highly efficient 16% overall yield.

The synthesis of the A-ring subunit of bryostatin 1 (Fig. 3, acid **1**) began with the condensation of *t*-butyl acetate and propionate **19**, a rare example of a Claisen reaction between two enolizable coupling partners. We found that sterically large substituents on both the electrophile (i.e., 3,3-diethoxy groups) and nucleophile (*t*-butyl group) were necessary to suppress enolate exchange events leading to undesired products. The resultant β-ketoester **20** was reduced with Noyori's catalyst (96% ee) and straightforwardly converted to aldehyde

21. This three-step sequence from **19** to **21** was routinely carried out on 30-g batches with one chromatographic purification in a single week (~80% yield per step).

Aldehyde **21** was combined with β-diketone **22** in a substrate-controlled boron aldol reaction to afford hydroxyketone **23** in equilibrium with its hemiketal isomer (86% combined yield, 2:1 dr). Alternative aldol methods failed to selectively deliver the 1,3-*anti* adduct. For example, Paterson's diisopinocampheyl (Ipc) protocol (38) led only to reduction (39) of the C9 carbonyl group of β-diketone **22**, whereas Mukaiyama (Lewis acids: BF_3, $AlMe_2Cl$, $TiCl_4$, $SnCl_4$, Tf_2NH) and metal-enolate reactions (Li, Zn, Sm) generally gave complex mixtures that were at best ~1:1 dr. Notwithstanding the moderate 2:1 selectivity for this boron aldol reaction, this process was selected for use because of its favorable throughput on multigram scales.

The chemo- and diastereoselective reduction of C7 ketone **23** was accomplished by modifying standard Evans-Saksena reaction conditions (40). We found that application of either Me_4N- or $NaBH(OAc)_3$ in AcOH/MeCN resulted in low diastereoselectivity (2:1 dr); however, after the introduction of acetone as a co-solvent, which likely suppressed intermolecular reduction events, the dr improved to >15:1. Ketalization at C9 (using trimethylorthoformate as a dehydrating agent), followed by a one-flask acylation at C7 and chemoselective acetal hydrolysis (41) at C11, then afforded aldehyde **25**.

The diastereoselective allylation of aldehyde **25** proceeded in 84% yield and 10:1 dr (decagram scale) using Leighton's chiral diamine controller with silane **26** (42). The high efficiency of this Leighton allylation belies the many difficulties we experienced in surveying allylation platforms, most of which could not be extended to incorporate the sensitive trimethylsilyl moiety [e.g., Ipc method (43)] or did not react with the highly oxygenated and β-disubstituted aldehyde **25** [e.g., chiral allylstannane platforms (44, 45)]. Silylation of the C11 alcohol and hydrolysis of the C1 ester (46) then completed the A-ring subunit, **1**, in 13% overall yield (10 steps).

A Yamaguchi esterification united the A- and C-ring fragments, **1** and **2**, in 82% yield (Fig. 4A) and set the stage for another key step, a Prins macrocyclization (28, 47). Catalyzed by pyridinium *p*-toluenesulfonate (PPTS) in methanol, this process formed bryostatin's B-ring while closing the macrocycle (76% yield of **29** and 11% yield of C26 desilylated product). The resultant macro-lactone incorporating four different π-systems served as a third test of our selective alkene oxidation plan. Gratifyingly, a stoichiometric ozonolysis of **29** occurred chemoselectively to yield ketone **30** [80% yield, 90% based on recovered starting material (brsm)]. We found that by performing this reaction in the presence of methanol (versus dichloromethane alone), the yield increased from ~50% to 80%, likely by mitigating the negative effects arising from ionization of the C9 ketal.

At this point, the long-deferred alkynoate-to-diene isomerization was ready to be tested. Using a modification of a procedure reported by Rychnovsky (48), the C20 ynoate of **30** was isomerized with triphenylphosphine and 2,4,6-trimethylphenol to afford dienoate **31** in 90% yield. This practical and efficient conversion ranks among the most complex examples of an ynoate isomerization process reported to date (49).

The B-ring enoate was installed by a Horner-Wadsworth-Emmons reaction using Fuji's phosphonate **32** (21, 50). We found that this 3,3′-dimethyl-BINOL phosphonate gave a significantly higher *Z:E* ratio than the corresponding unsubstituted reagent (11:1 vs. 3:1 *Z:E*). Finally, the silyl ethers and C9 ketal of **33** were cleaved with buffered HF-pyridine followed by in situ hydrolysis to yield bryostatin 1 in 80% yield (30% overall yield from aldehyde **2**). This synthetic product was >99.5% pure after high-performance liquid chromatography purification and crystallization (CH_2Cl_2/MeOH). In all analytical respects, including nuclear magnetic resonance and infrared spectroscopies, optical rotation, and high-resolution mass spectrometry, synthetic bryostatin 1 was identical to an authentic sample of natural bryostatin 1 supplied by the NCI. To further validate the structure of the synthetic material, we determined a crystal structure of synthetic bryostatin 1 (Fig. 1) by x-ray diffraction.

This study opens practical, gram-scale access to bryostatin 1 and a wide range of analogs derivable from late-stage intermediates. For example, derivatives **34** and **35** (Fig. 4B), which feature structural variations of bryostatin's B-ring, were each accessed in one step from late-stage intermediates. The B-ring is of potential importance because our group has recently shown in long–time scale (400 to 500 μs) molecular dynamics simulations that the hydrogen-bonding network imposed by bryostatin's A- and B-rings can stabilize an otherwise transient state of its protein target, PKC, thereby providing a rationalization for bryostatin's unique biological activity (51). Analogs **34** and **35** exhibited low nanomolar affinity to PKC-βI and PKC-δ, representative conventional and novel PKC isoforms, respectively (Fig. 4C). However, these compounds displayed different isoform selectivities relative to bryostatin 1, which binds all conventional and novel PKC isoforms with single-digit nanomolar affinity. Because different isoforms are associated with different therapeutic indications, access to isoform-selective PKC modulators enables the development of more therapeutically relevant, disease-specific leads (5, 6, 52, 53). This work opens sustainable research access to bryostatin 1 as well as more synthetically accessible analogs that are proving to be more effective and better tolerated in comparative studies with cells, disease models in animals, and ex vivo samples taken from HIV-positive patients (27, 54).

Supplementary Material

Refer to Web version on PubMed Central for supplementary material.

Acknowledgments

Supported by American Cancer Society Postdoctoral Fellowship PF-15-007-01-CDD (S.H.), NSF Graduate Research Fellowships (R.V.Q., A.J.S., M.C.S.), NSF award ECCS-1542152 (for use of the Stanford Nano Shared Facilities), NIH grant P30 CA124435 (for use of the Stanford Cancer Institute Proteomics/Mass Spectrometry Shared Resource), and NIH grants R01CA031845 and AI124743. We thank the NCI for graciously providing a sample of natural bryostatin 1 and the Vincent Coates Foundation Mass Spectrometry Laboratory, Stanford University Mass Spectrometry (https://mass-spec.stanford.edu). Q. H. Luu-Nguyen and J. H. Tyler have recently repeated and in places improved upon early scaled steps. Stanford University has filed a provisional patent application (application serial no. 62/404,687) on this technology, which has been licensed by Neurotrope BioScience for the treatment of neurological disorders. An option to license has been granted by Stanford University to Bryologx Inc. for use in HIV/AIDS eradication and cancer immunotherapy. P.A.W. is an adviser to both companies and a cofounder of the latter. Structural parameters for bryostatin 1 are available free of charge from the Cambridge Crystallographic Data Centre under CCDC-1564674. All additional relevant data are included in the supplementary materials.

REFERENCES AND NOTES

1. Gutiérrez C, et al. AIDS. 2016; 30:1385–1392. [PubMed: 26891037]
2. Bullen CK, Laird GM, Durand CM, Siliciano JD, Siliciano RF. Nat Med. 2014; 20:425–429. [PubMed: 24658076]
3. Laird GM, et al. J Clin Invest. 2015; 125:1901–1912. [PubMed: 25822022]
4. A Study Assessing Bryostatin in the Treatment of Moderately Severe to Severe Alzheimer's Disease. https://clinicaltrials.gov/ct2/show/NCT02431468
5. Nelson TJ, et al. J Alzheimers Dis. 2017; 58:521–535. [PubMed: 28482641]
6. Alfonso SI, et al. Sci Signal. 2016; 9:ra47. [PubMed: 27165780]
7. Hammond C, et al. J Immunother. 2005; 28:28–39. [PubMed: 15614042]
8. Shaha SP, et al. Clin Exp Immunol. 2009; 158:186–198. [PubMed: 19737143]
9. Kortmansky J, Schwartz GK. Cancer Invest. 2003; 21:924–936. [PubMed: 14735696]
10. Mochly-Rosen D, Das K, Grimes KV. Nat Rev Drug Discov. 2012; 11:937–957. [PubMed: 23197040]
11. Barr PM, et al. Am J Hematol. 2009; 84:484–487. [PubMed: 19536846]
12. Pettit GR, et al. J Am Chem Soc. 1982; 104:6846–6848.
13. Pettit GR, Day JF, Hartwell JL, Wood HB. Nature. 1970; 227:962–963. [PubMed: 4393654]
14. Schaufelberger DE, et al. J Nat Prod. 1991; 54:1265–1270. [PubMed: 1800630]
15. Castor, TP. US Patent. 5750709 A. 1998.
16. Keough MJ. Biol Bull. 1989; 177:277–286.
17. Mendola D. Biomol Eng. 2003; 20:441–458. [PubMed: 12919831]
18. Trindade-Silva AE, Lim-Fong GE, Sharp KH, Haygood MG. Curr Opin Biotechnol. 2010; 21:834–842. [PubMed: 20971628]
19. Miller IJ, Vanee N, Fong SS, Lim-Fong GE, Kwan JC. Appl Environ Microbiol. 2016; 82:6573–6583. [PubMed: 27590822]
20. Kageyama M, et al. J Am Chem Soc. 1990; 112:7407–7408.
21. Evans DA, et al. J Am Chem Soc. 1999; 121:7540–7552.
22. Ohmori K, et al. Angew Chem Int Ed. 2000; 39:2290–2294.
23. Trost BM, Dong G. Nature. 2008; 456:485–488. [PubMed: 19037312]
24. Keck GE, Poudel YB, Cummins TJ, Rudra A, Covel JA. J Am Chem Soc. 2011; 133:744–747. [PubMed: 21175177]
25. Wender PA, Schrier AJ. J Am Chem Soc. 2011; 133:9228–9231. [PubMed: 21618969]
26. Lu Y, Woo SK, Krische MJ. J Am Chem Soc. 2011; 133:13876–13879. [PubMed: 21780806]
27. Wender PA, et al. J Am Chem Soc. 2002; 124:13648–13649. [PubMed: 12431074]
28. Wender PA, Dechristopher BA, Schrier AJ. J Am Chem Soc. 2008; 130:6658–6659. [PubMed: 18452292]
29. DeChristopher BA, et al. Nat Chem. 2012; 4:705–710. [PubMed: 22914190]
30. Wender PA, et al. Proc Natl Acad Sci USA. 1988; 85:7197–7201. [PubMed: 3174627]
31. Cheng HS, Loh TP. J Am Chem Soc. 2003; 125:4990–4991. [PubMed: 12708844]
32. Nokami J, et al. J Am Chem Soc. 2001; 123:9168–9169. [PubMed: 11552828]
33. Hale KJ, Frigerio M, Manaviazar S. Org Lett. 2003; 5:503–505. [PubMed: 12583754]
34. Keck GE, Truong AP. Org Lett. 2005; 7:2149–2152. [PubMed: 15901156]
35. Trost BM, Yang H, Dong G. Chemistry. 2011; 17:9789–9805. [PubMed: 21780195]
36. Valenta P, Drucker NA, Bode JW, Walsh PJ. Org Lett. 2009; 11:2117–2119. [PubMed: 19419211]
37. Imamoto T, et al. J Org Chem. 1984; 49:3904–3912.
38. Paterson I, et al. Tetrahedron. 1990; 46:4663–4684.
39. Brown HC, Chandrasekharan J, Ramachandran PV. J Am Chem Soc. 1988; 110:1539–1546.
40. Evans DA, Chapman KT, Carreira EM. J Am Chem Soc. 1988; 110:3560–3578.
41. Fujioka H, et al. J Am Chem Soc. 2006; 128:5930–5938. [PubMed: 16637661]

42. Suen LM, Steigerwald ML, Leighton JL. Chem Sci. 2013; 4:2413–2417. [PubMed: 25165504]
43. Srebnik M, Ramachandran PV. ChemInform. 1987; 20:9.
44. Keck GE, Covel JA, Schiff T, Yu T. Org Lett. 2002; 4:1189–1192. [PubMed: 11922815]
45. Yu CM, Lee JY, So B, Hong J. Angew Chem Int Ed. 2002; 41:161–163.
46. Nicolaou KC, Estrada AA, Zak M, Lee SH, Safina BS. Angew Chem Int Ed. 2005; 44:1378–1382.
47. Han X, Peh G, Floreancig PE. Eur J Org Chem. 2013; 2013:1193–1208.
48. Rychnovsky SD, Kim J. J Org Chem. 1994; 59:2659–2660.
49. Kwong CKW, Fu MY, La CSL, Toy PH. Synthesis. 2008; 15:2307–2317.
50. Tanaka K, Ohta Y, Fuji K, Taga T. Tetrahedron Lett. 1993; 34:4071–4074.
51. Ryckbosch SM, Wender PA, Pande VS. Nat Commun. 2017; 8:6. [PubMed: 28232750]
52. Trushin SA, et al. J Virol. 2005; 79:9821–9830. [PubMed: 16014943]
53. McKernan LN, Momjian D, Kulkosky J. Adv Virol. 2012; 2012:805347. [PubMed: 22500169]
54. Wender, PA., Donnelly, AC., Loy, BA., Near, KE., Staveness, D. Natural Products in Medicinal Chemistry. Wiley-VCH; 2014. p. 473-544.

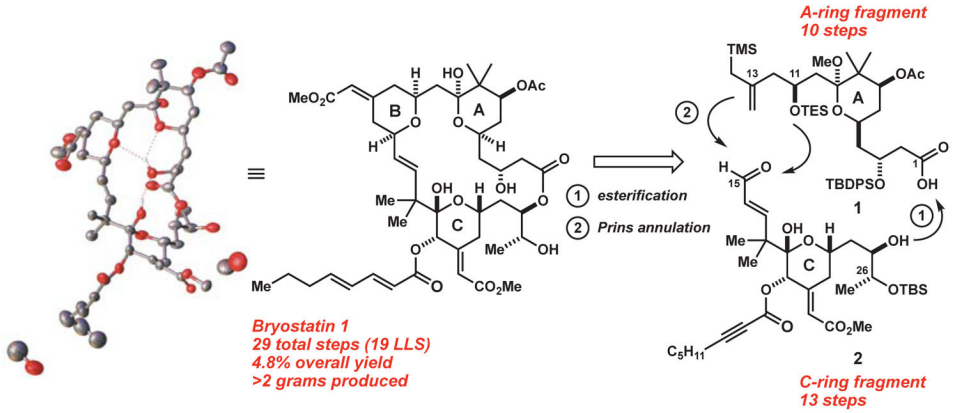

Fig. 1.

Retrosynthetic analysis of bryostatin 1, and its crystal structure (with bound methanol) determined by x-ray diffraction.

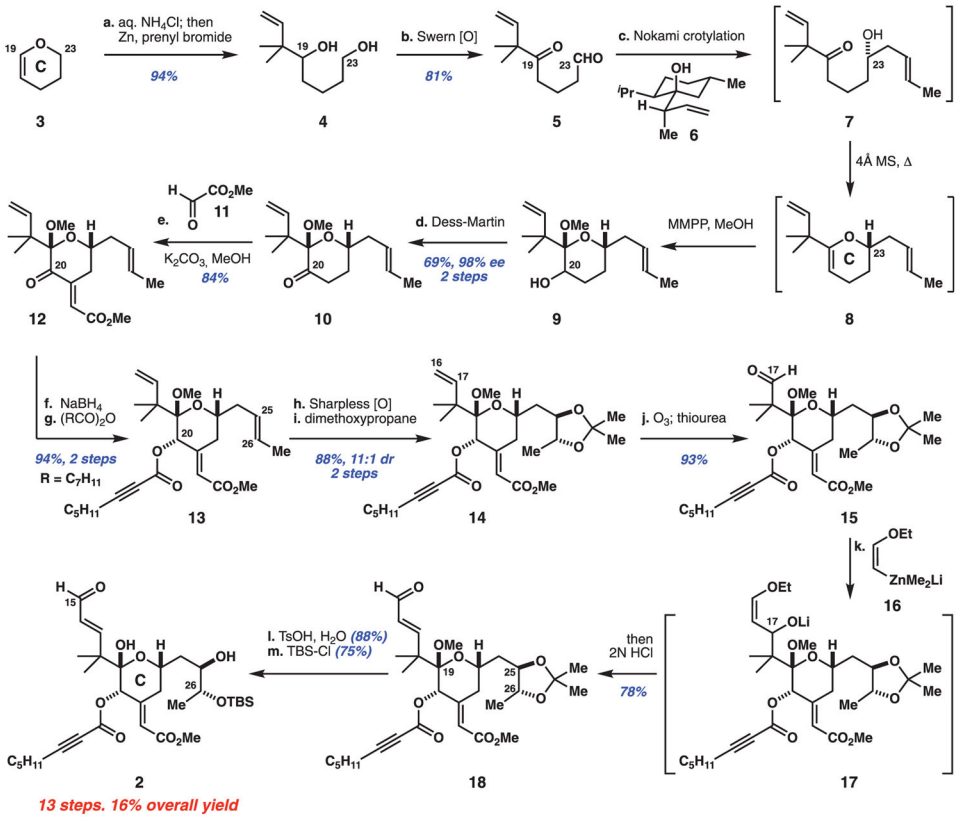

Fig. 2. Reaction sequence for the C-ring subunit, 2

Reagents and conditions: **a.** NH_4Cl, H_2O; then zinc powder (3.4 equiv), prenyl bromide (1.7 equiv), tetrahydrofuran (THF). **b.** Oxalyl chloride (3 equiv), dimethyl sulfoxide (DMSO) (4 equiv), CH_2Cl_2, −78°C; then **4**; then Et_3N (8 equiv), −78° to −30°C. **c.** Reagent **6** (2 equiv), *p*-toluenesulfonic acid (*p*-TsOH-H_2O) (10 mol %), $CHCl_3$; then 4 Å molecular sieves, 70°C; then magnesium monoperoxyphthalate (MMPP) hexahydrate (0.45 equiv), $NaHCO_3$ (2 equiv), MeOH, 0°C. **d.** Dess-Martin periodinane (1.5 equiv), pyridine (10 equiv), CH_2Cl_2, 0°C. **e.** Glyoxylate **11** (5 equiv), K_2CO_3 (5.5 equiv), 4.4:1 THF/MeOH. **f.** $CeCl_3$-$7H_2O$ (0.5 equiv), $NaBH_4$ (2 equiv), MeOH, −50°C. **g.** $(C_7H_{11}CO)_2O$ (3 equiv), 4-dimethylaminopyridine (DMAP) (1 equiv), CH_2Cl_2, −20° to 0°C. **h.** $K_2OsO_2(OH)_4$ (1 mol %), dihydroquinidine 1,4-phthalazinediyl diether $(DHQD)_2PHAL$ (5 mol %), $K_3Fe(CN)_6$ (3 equiv), K_2CO_3 (3 equiv), $MeSO_2NH_2$ (1 equiv), 1:1 *t*-BuOH/H_2O, 0°C. **i.** 2,2-Dimethoxypropane (4 equiv), PPTS (10 mol %), CH_2Cl_2. **j.** Ozone (~1.8 equiv), CH_2Cl_2, −78°C; then thiourea (10 equiv), *i*-PrOH, −78°C to room temperature. **k.** *Cis*-1-bromo-2-ethoxyethylene (8 equiv), *t*-BuLi (16 equiv), Me_2Zn (8.8 equiv), Et_2O, −78°C; then aldehyde **15**; then 1M HCl (64 equiv). **l.** *p*-TsOH-H_2O (1 equiv), 4:1 MeCN/H_2O, room temperature to 45°C. **m.** *t*-Butyldimethylsilyl chloride (TBS-Cl) (1.5 equiv), imidazole (2 equiv), *N*,*N*-dimethylformamide (DMF). Me, methyl; Et, ethyl; Bu, butyl.

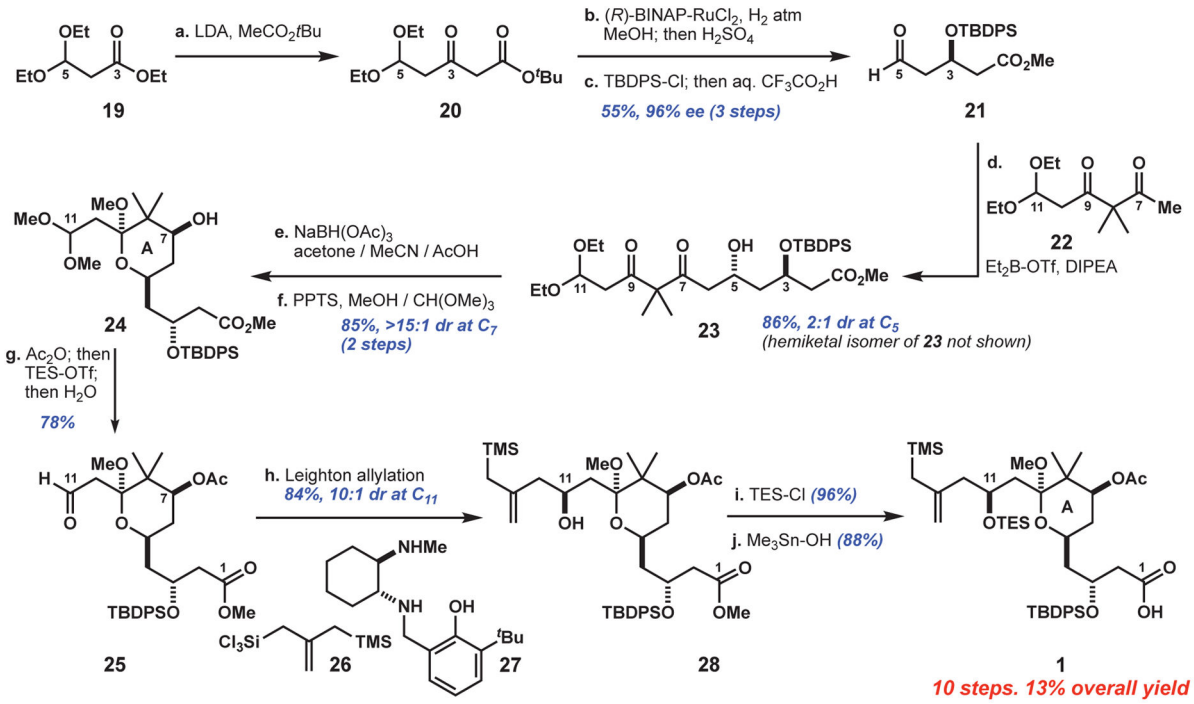

Fig. 3. Reaction sequence for the A-ring subunit, 1

Reagents and conditions: **a.** *n*-BuLi (4 equiv), *i*-Pr_2NH (4.1 equiv), THF, −78°C; then *t*-butyl acetate (4.05 equiv); then **19** (1 equiv), −78°C to room temperature. **b.** (*R*)-BINAP-$RuCl_2$ (0.4 mol %), H_2 (650 psi), MeOH, 45°C; then H_2SO_4 (7.5 mol%), 60°C. **c.** *t*-Butyldiphenylsilyl chloride (TBDPS-Cl) (1 equiv), imidazole (1.5 equiv), CH_2Cl_2; then 1:1 H_2O:CF_3CO_2H, 0°C. **d.** Ketone **22** (2 equiv), diethylboron triflate (Et_2B-OTf) (1.95 equiv), *i*-Pr_2EtN (2 equiv), Et_2O, −78°C; then aldehyde **21** (1 equiv), pentane. **e.** Sodium triacetoxyborohydride (7 equiv), 1:2:3 MeCN/acetone/AcOH, 0°C to room temperature. **f.** Pyridinium *p*-toluenesulfonate (PPTS) (1 equiv), 4:1 MeOH/$CH(OMe)_3$. **g.** Acetic anhydride (Ac_2O) (1.1 equiv), DMAP (10 mol %), 2,4,6-trimethylpyridine (9 equiv), CH_2Cl_2, −40°C; then triethylsilyl trifluoromethanesulfonate (TES-OTf) (5.5 equiv); then H_2O, −40° to 0°C. **h.** Silane **26** (1.6 equiv), diaminophenol **27** (1.2 equiv), 1,8-diazabicyclo[5.4.0]undec-7-ene (DBU) (3.6 equiv), CH_2Cl_2, 0°C to room temperature; then aldehyde **25**, −78°C; then tetrabutylammonium fluoride (TBAF) (1 equiv). **i.** Triethylsilyl chloride (TES-Cl) (1.5 equiv), imidazole (6 equiv), CH_2Cl_2, 0°C. **j.** Me_3Sn-OH (3.5 equiv), toluene, 85°C; then Ac_2O (5 equiv), DMAP (6 equiv), 0°C; then H_2O, 0°C to room temperature.

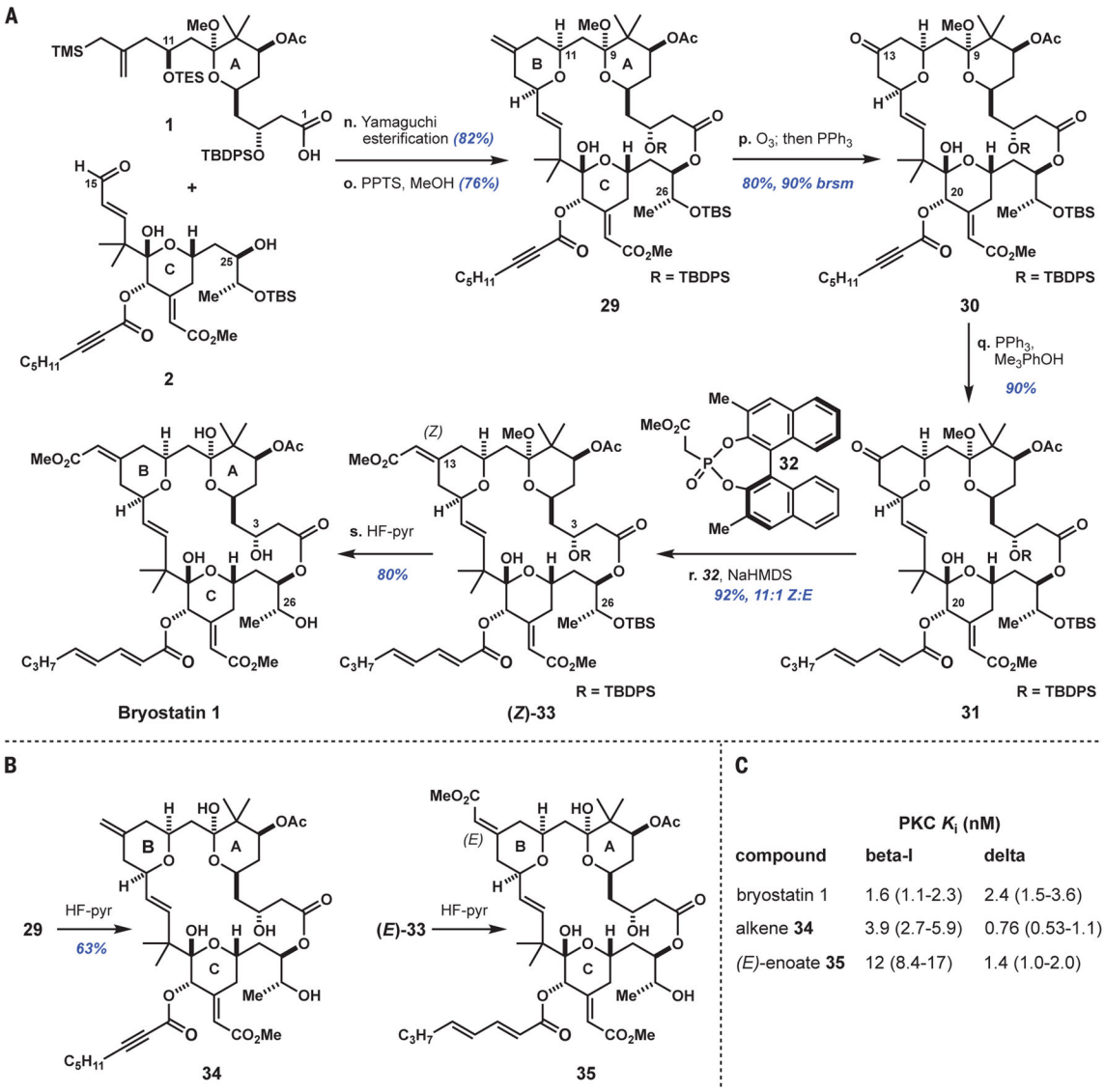

Fig. 4. Completion of bryostatin 1 synthesis and one-step diversifications toward analog compounds

(**A**) Reaction sequence for bryostatin 1; (**B**) synthesis of derivatives **34** and **35**; (**C**) characteristics of **34** and **35** versus bryostatin 1. Reagents and conditions: **n.** Acid **1** (1 equiv), 2,4,6-trichlorobenzoyl chloride (1.8 equiv), Et_3N (6 equiv), toluene; then alcohol **2** (1 equiv), DMAP (3 equiv). **o.** PPTS (30 mol %), 50:1 MeOH/$CH(OMe)_3$. **p.** Ozone (~1.9 equiv), MeOH/CH_2Cl_2, −78°C; then triphenylphosphine (Ph_3P) (2 equiv), −78°C to room temperature. **q.** Ph_3P (5 equiv), 2,4,6-trimethylphenol (5 equiv), benzene. **r.** Phosphonate **32** (14 equiv), sodium hexamethyldisilazide (NaHMDS) (13 equiv), THF, −78° to 4°C. **s.** 1:2:2 HF-pyridine/pyridine/THF, 40°C; then H_2O, 40°C. See supplementary materials for PKC binding assay protocol. Error ranges in parentheses indicate 95% confidence intervals from nonlinear regression analysis.